Theoretical Validation of Chemical Kinetic Mechanisms: Combustion of Methanol

ARTICLE *in* THE JOURNAL OF PHYSICAL CHEMISTRY A · AUGUST 2010

Impact Factor: 2.69 · DOI: 10.1021/jp1047002 · Source: PubMed

5 AUTHORS, INCLUDING:

Alison Tomlin
University of Leeds
143 PUBLICATIONS **2,304** CITATIONS

Theoretical Validation of Chemical Kinetic Mechanisms: Combustion of Methanol

Rex T. Skodje,*,†,‡ Alison S. Tomlin,§ Stephen J. Klippenstein,‡ Lawrence B. Harding,‡ and Michael J. Davis‡

Department of Chemistry and Biochemistry, University of Colorado, Boulder, Colorado 80309-0215, School of Process, Environmental and Materials Engineering, University of Leeds, Leeds LS2 9JT, U.K., and Chemical Sciences and Engineering Division, Argonne National Laboratory, Argonne, Illinois 60439

Received: May 21, 2010; Revised Manuscript Received: June 30, 2010

A new technique is proposed that uses theoretical methods to systematically improve the performance of chemical kinetic mechanisms. Using a screening method, the chemical reaction steps that most strongly influence a given kinetic observable are identified. The associated rate coefficients are then improved by high-level quantum chemistry and transition-state-theory calculations, which leads to new values for the coefficients and smaller uncertainty ranges. This updating process is continued as new reactions emerge as the most important steps in the target observable. The screening process employed is a global sensitivity analysis that involves Monte Carlo sampling of the full *N*-dimensional uncertainty space of rate coefficients, where *N* is the number of reaction steps. The method is applied to the methanol combustion mechanism of Li et al. (*Int. J. Chem. Kinet.* **2007**, *39*, 109.). It was found that the $CH_3OH + HO_2$ and $CH_3OH + O_2$ reactions were the most important steps in setting the ignition delay time, and the rate coefficients for these reactions were updated. The ignition time is significantly changed for a broad range of high-concentration methanol/oxygen mixtures in the updated mechanism.

I. Introduction

The use of theoretical kinetic modeling provides an invaluable tool for the study of a variety of complicated chemical problems ranging from fuel combustion to atmospheric chemistry to surface catalysis.[1] Such models generally consist of a set of *N* elementary chemical reaction steps that are quantitatively described by the reaction rate coefficients, k_i, $i = 1, ..., N$, together with a description of the thermodynamic and transport properties. Often, the choice of reactions and certain values of the rate coefficients are adjusted to reproduce experimental observations for a validation data set obtained for some range of conditions. For chemical modeling to have predictive value, the k_i must be known to sufficient accuracy to give the desired system properties over an even wider range of conditions than provided by the validation set. For the case of a sufficiently simple chemical mechanism, there are relatively few rate coefficients, and these can, in principle, be directly determined through experiment. Unfortunately, for most realistic problems, there are too many elementary steps for an accurate experimental determination of all of the k_i. This is particularly true for combustion mechanisms of complicated fuels wherein a hierarchical construction generates a description of the *n*-carbon system by augmenting the mechanism for the $(n - 1)$-carbon system; that is, methane $\subset$ ethane $\subset$ propane, and so on. The Lawrence Livermore *n*-heptane mechanism already consists of 2539 reactions and 561 distinct species.[2] In addition to the sheer number of elementary reactions, direct measurement of k_i is complicated by the circular need for theoretical modeling to extract the result from experiment. As a consequence, many of the rate coefficients for complicated combustion mechanisms are instead provided by simple rules of a mechanism generation method such as group additivity.[3] The uncertainty range of rate coefficients obtained in such fashion can be quite large. Indeed, it is not unusual for the uncertainty ratio $\log(|\Delta k_i/k_i|)$ to be of order 1 (i.e., a factor of 10). Given such huge inaccuracy in the description of the chemistry, it is not surprising that the performance of large models can break down badly when applied outside the range of conditions for which the model has been optimized.

The objective of the present work is to advance a method to improve the performance of chemical models that have proven unsatisfactory because of the inaccuracy of the rate coefficients. Whereas a given k_i value has traditionally been improved by new experimental measurements, herein, we propose a scheme that employs the methods of theoretical chemistry. Specifically, the reaction barrier (or effective dynamical bottleneck) is first characterized using high-level quantum chemistry calculations; k_i is subsequently generated from this information using transition-state theory (TST) or Rice−Ramsperger−Kassel−Marcus (RRKM) theory. It is known that theoretical rate coefficients can be quite accurate when the computational methods are applied with the highest level of sophistication. One expects that k_i values computed in this way should be much more reliable than rule-generated k_i values. Unfortunately, such high-level computations are quite intensive and cannot be carried out indiscriminately for all of the reactions of a large mechanism. Therefore, the essential element of our method is a procedure to identify the key reaction steps of the mechanism that are targeted for high-level computation. The key reactions are identified, and the k_i values recomputed, in a sequential fashion so that the performance of the model is progressively improved one reaction at a time. In this way, we hope that a satisfactory model can be generated with a relatively modest number of calculations of rate coefficients. We should point out that mechanism improvement methods have been proposed previ-

* To whom correspondence should be addressed. E-mail: Rex.Skodje@colorado.edu.
† University of Colorado.
‡ Argonne National Laboratory.
§ University of Leeds.

10.1021/jp1047002
Published on Web 07/23/2010

ously that involve the use of sensitivity analysis.[4,5] We note that one unique aspect of the present work is the use of theoretical methods, as opposed to an experimental approach, to improve the rate coefficients. Furthermore, our primary objective is to produce models with lower uncertainties rather than to optimize the agreement between predictions and experiment. If we were to attempt such model−experiment optimization, then it would be advisible to account for uncertainties in the experimental observations themselves.[6]

To identify the key reaction steps of a mechanism, we make use of global screening methods that have been developed by the statistics community to locate the important variables (or factors) in high-dimensional response functions.[7] As discussed in detail in section II, the "importance" of a given reaction step in affecting an observed quantity (the response function) is a composite of two characteristics: first, the intrinsic sensitivity of the response function to k_i and, second, the uncertainty range of k_i.[8] Thus, for example, an observable quantity might be highly sensitive to a given k_i, but yet k_i might not be targeted for improvement because Δk_i might already be quite small. The largest payoff will be obtained by computing a rate coefficient to which the target observable is highly sensitive and which is also highly uncertain. We should distinguish global screening methods from traditional chemical diagnostics, such as local sensitivity analysis, which do not reflect the uncertainty of knowledge of rate constants. It is possible to combine the local sensitivity coefficient, s_i, with the uncertainty range to obtain an estimate of the overall uncertainty through the parameter $\Delta k_i s_i$.[9] However, when the response of the kinetics to the rate coefficients is highly nonlinear, such local schemes can be quite misleading (see Figure 1 below). Global sensitivity or uncertainty analysis has been discussed in the chemical kinetics literature for many years, but has not been routinely applied to large mechanisms, in part, because of the computational demands of exploring large regions of factor space.[8−21]

We are interested in improving mechanisms used to analyze the combustion of oxygenated fuels, which have become the subject of increasing attention because of the recent attention to the study of biofuels. Alcohols have been the most common examples of biofuels and have been the subject of considerable interest.[22] Here, we focus on the chemical kinetics of the burning of methanol (and methanol blends in future work) as the simplest alcohol. Although the methanol system represents neither the optimal biofuel surrogate nor the most highly uncertain combustion mechanism, it does provide a good test problem to demonstrate the power of our mechanism improvement scheme for a modestly sized system. We also point out that, in the spirit of hierarchical model development, the optimized methanol mechanism will become part of the mechanism for more complicated fuels.

Li et al.[23] recently proposed a kinetic mechanism to describe the combustion of CH_3OH, CH_2O, and/or CO that involves 93 reversible reactions and 18 chemical species (excluding inert buffer gases). Comparisons of experimentally obtained laminar flame speeds and ignition delay times to model predictions showed a good pattern of agreement. We point out, however, that the experiments were carried out at low concentrations, thus leaving open the possibility of model failure for high-concentration/high-pressure conditions appropriate to engine combustion. In the present work, we focus on mechanism improvement for the engine conditions for which experimental validation is lacking. Of primary concern here is the early-stage kinetics that is reflected by the ignition delay time.[24] We should expect that this choice will tend to emphasize distinct aspects of the mechanism that might differ from those emphasized with other choices such as the flame speed.

This article is organized as follows: In section II, we begin by outlining the basic procedures and strategies in our mechanism improvement method. The global screening methodology is then presented in detail and adapted to the problem of combustion modeling. The methods used to update the rate coefficients are then briefly reviewed. Anticipating the outcome of the screening analysis, the computations on the reactions $CH_3OH + HO_2$ and $CH_3OH + O_2$ are then discussed. In section III, the results of numerical calculations are presented. Two updates are performed on the rate coefficients, leading to stage 2 and stage 3 mechanisms. The influence of the updates on the original experimental validation set is discussed. Finally, in section IV, the conclusions from the work are drawn.

A brief report of parts of this work was provided previously where the emphasis was on the theoretical analysis of the elementary reaction kinetics and its affect on the ignition delay for one particular set of initial conditions.[25] In this study, we provide a much more detailed description of the uncertainty screening and also consider the application to a wide range of initial conditions. We also alert the reader that similar analyses of the combustion of H_2[26] and of butanol[27] are presently being undertaken.

II. Method

The outline for the mechanism improvement strategy we propose is straightforward. We begin with the presumption that a nominal mechanism exists for the system of interest composed of N chemical steps with given rate coefficients k_i and that estimates for the uncertainties in the rate coefficients, Δk_i, are available. Uncertainties might also exist in other model parameters, such as thermochemical data, which, if quantified, can also be addressed on an equal footing by our method. Given this, the method consists of the following steps:

Step 1. We identify an observable target that we want the theoretical mechanism to accurately reproduce. For autoignition in a diesel engine, a good choice of target is the ignition delay time (τ), which is the time required for the fuel/O_2 mixture to ignite under the desired (T, P) initial engine conditions. The response surface is then the target as a function of the rate coefficient factors, $\tau(k_1,k_2, ..., k_N)$; thus, τ is a very high-dimensional function that is sensitive to the ignition properties.

Step 2. Using screening methods developed largely in the statistics literature, we identify the rate constants that most strongly influence the target. We assume that the uncertainties in k_i are large, and thus, the screening process must be global in nature.[28] This requires repeated calculation of the target function at various points within the N-dimensional uncertainty range of k_i values. For typical combustion mechanisms, this statistical sampling requires the time integration of the kinetics equations for thousands of choices of the rate coefficients. As discussed in detail below, the statistical sample is used to compute the main effect, or first-order sensitivity index, which is a measure of the contribution of a single factor, k_i, to the variation of the target within the uncertainty range. It is critical to realize that there are two quantities that determine the magnitude of the main effect: first, the intrinsic sensitivity of τ to the variable k_i and, second, the magnitude of the uncertainty range of k_i, that is, Δk_i. For complicated fuels, $\Delta k_i/k_i$ can be a factor of 10 or larger. Notably, a reaction for which τ is very sensitive might nevertheless be unimportant (small main effect) if the corresponding k_i value is known very accurately.

Step 3. The reaction with the largest main effect from step 2 is selected for improvement. The objective is to improve the

value of the rate coefficient and to reduce the uncertainty, Δk_i, so that the main effect becomes smaller. Although, in principle, experiments can be done to find the rate constant,[4] we shall instead use theoretical calculations to determine k_i. The barrier and (perhaps) the reaction path for the reaction in question are analyzed using quantum chemistry calculations. At minimum, it is necessary to compute the energy, geometry, and normal-mode frequencies at the saddlepoint and the reactant potential minimum. These inputs are required for conventional TST calculations. Under some circumstances, such as when the barrier is low, the dynamical bottleneck can migrate away from the saddlepoint.[29] For variational TST (i.e., VTST), the computation of the reaction path and frequencies of the projected force constant matrix are also necessary to locate the new bottleneck and compute the rate coefficient.[30] The properties of the reaction path (at least the imaginary frequency) are also needed if a determination of the tunneling transmission coefficient is desired.[31] The TST calculation yields a new $k(T)$ value, and internal consistency checks on the quantum chemistry, combined with experience with ab initio transition-state theory methodologies, suggests a new, presumably smaller, estimate for Δk_i.

Step 4. Once the most important reaction rate constant (largest main effect) has been improved through step 3, the response surface is recalculated using the new mechanism. Assuming that the uncertainty range of the selected reaction is sufficiently reduced, the new simulation will uncover a new reaction with the largest main effect. Step 3 is then repeated to improve that rate constant. This process continues until the uncertainty in the mechanism is reduced to an acceptable level.

Step 5 (Optional). Given that a mechanism is improved as much as practically possible using this method outlined above, a new target variable can be selected. This new target might be sensitive to different characteristics of the chemistry than is the original response surface. For example, the laminar flame speed target, which is most dependent on the later-stage steady-state properties of the flame, might serve as a good complement to short-time ignition properties reflected by τ.

In the remaining portion of this section, we present further details of this approach.

A. Screening Methods. The influence of a given factor (in our case, a rate coefficient) in a response surface can be determined using a screening method.[7] For our purposes, the screening process is useful in identifying which of the k_i values should be selected for improvement. Obviously, the results of the screening process will depend, at least to some degree, on the choice of the response function. This selection must be guided by physical insight and the uses envisioned for the chemical model. In the present work, we are interested in the ignition properties of methanol. Therefore, we select the ignition delay time as our response surface

$$\tau = \tau(k_1, k_2, ..., k_N) \tag{2.1}$$

which is a scalar function of the N input factors. The details of the computation will be discussed below, and for present, we simply point out that τ is determined by numerical integration of the kinetics equations from fixed initial conditions (temperature, pressure, initial concentrations of reagents) and that no "measurement error" is accrued. Thus, τ is assumed to be a smooth deterministic function with only a very small numerical integration error.

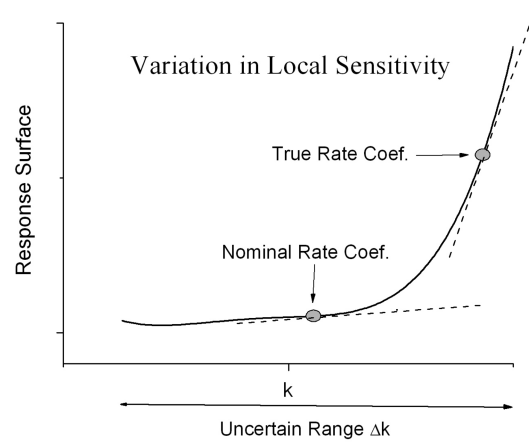

Figure 1. Schematic diagram showing the response surface (solid line), which is a highly nonlinear function of the rate coefficient k. The local sensitivities, measured by the slopes of the dashed lines, are seen to be extremely different at the nominal value and the "true" value.

In traditional chemical modeling, it is common to assess the importance of a given reaction by computing the local sensitivity coefficients[32,33]

$$s_i = \left.\frac{\partial \ln \tau}{\partial \ln k_i}\right|_{\mathbf{k}=\mathbf{k}_0} \tag{2.2}$$

where $\mathbf{k}_0$ represents the rate coefficients for the nominal mechanism. As illustrated in Figure 1, we see that the slope, reflected through s_i, can provide a very poor screening measure when the uncertainty range of the factors becomes large. In this one-dimensional schematic, we see that the local sensitivity coefficient is small at the nominal mechanism but is very large at the "true" mechanism. Other important nonlinear behavior of τ might also go unnoticed using s_i such as strong factor correlation. Even methods that employ global but highly sparse sampling of factor space can miss important aspects of the sensitivity. The distinction between local and global sensitivity analysis is well-known and has been investigated numerically in combustion models.[18,19,34]

A more satisfactory treatment is provided by an analysis of the variance function, which reflects the change in the response surface over the global uncertainty range. Uncertainty analysis, as typically defined, concerns the investigation of the distribution of values of τ obtained by varying the factors $\mathbf{k}$ over their uncertainty range. Global sensitivity analysis, on the other hand, is concerned with apportioning the variation of τ to specific factors and, thus, is apropos for a screening method. We assume that the N factors $\mathbf{k}$ are uncertain within a hypervolume of rate coefficient space, $\Omega = \Delta k_1 \times \Delta k_2 \times \cdots \times \Delta k_N$. Then, the total variance of τ within this space is

$$\sigma_T^2 = \langle \tau^2 \rangle - \langle \tau \rangle^2 = \int_\Omega P(\mathbf{k}) \tau^2 \, \mathrm{d}^N k - \tau_0^2 \tag{2.3}$$

where the mean is defined as $\langle \tau \rangle = \int_\Omega P(\mathbf{k}) \tau \, \mathrm{d}^N k \equiv \tau_0$ and $P(\mathbf{k})$ represents the probability distribution within the factor space. The function $P(\mathbf{k})$ is often set to 1, indicating a uniform distribution, although the forthcoming analysis requires only that it be separable, $P(\mathbf{k}) = \Pi P_i(k_i)$. The main effect (or first-order sensitivity index) of a given factor is a measure of the contribution to the variance from a single k_i assuming that the other factors are averaged over the uncertainty volume. A

reasonable definition of the main effect is the ratio of a "partial variance" to the total variance

$$S_i = \frac{{\sigma_i}^2}{{\sigma_T}^2} \tag{2.4}$$

We also point out that there are other global methods that do not rely on the analysis of variance such as that proposed by Morris.[35]

In this study, we compute the partial variance using a method inspired by the work of Sobol[36] that is closely related to the high-dimensional model representation (HDMR) developed by Rabitz and co-workers.[14,15,37−39] This approach is more numerically versatile than the method of Morris[35] and can be extended to the computation of correlated (or interaction) effects through higher-order sensitivity indices. The response surface is assumed to take the form of the expansion

$$\tau(k_1, k_2, ..., k_N) = \tau_0 + \sum_i A_i(k_i) + \sum_{i \neq j} B_{i,j}(k_i, k_j) + ... \tag{2.5}$$

In eq 2.5, τ_0 is the mean of τ, and the expansion is typically truncated after the first-order (A_i) or second-order ($B_{i,j}$) terms. Orthogonality constraints are imposed on the functions, which enforces the uniqueness of the expansion (or component) functions. Specifically, the relations $\langle A_i \rangle = \langle A_i A_j \rangle = \langle B_{n,m} \rangle = \langle A_i B_{n,m} \rangle = \cdots = 0$ will hold if the functions are written as expansions in orthogonal polynomials (see below for explicit formulas). The unknown functions are then defined rigorously through factor integration

$$\tau_0 + A_i(k_i) = \int_{\Omega'} P\tau \, \mathrm{d}^{N-1}k \quad i = 1, ..., N \tag{2.6a}$$

$$\tau_0 + A_i(k_i) + A_j(k_j) + B_{i,j}(k_i, k_j) = \int_{\Omega''} P\tau \, \mathrm{d}^{N-2}k \quad i \neq j = 1, ..., N \tag{2.6b}$$

where k_i is held constant in the integral 2.6a whereas k_i and k_j are held fixed in 2.6b. Once the expansion functions are determined, the partial variances are easily found by low-dimensional integration

$${\sigma_i}^2 = \int P_i(k_i) \, {A_i}^2(k_i) \, \mathrm{d}k_i \tag{2.7}$$

$${\sigma_{i,j}}^2 = \int P_i(k_i) \, P_j(k_j) \, {B_{i,j}}^2(k_i, k_j) \, \mathrm{d}k_i \, \mathrm{d}k_j \tag{2.8}$$

A significant improvement in efficiency is achieved if the unknown functions in eq 2.5 are evaluated using a numerical fitting procedure rather than direct integration. Thus, the hypervolume Ω is sampled by a large number, M, of vectors $\mathbf{k}$ according to the probability function $P(\mathbf{k})$ at which the response surface is evaluated to form the data set (k_j, τ_j), $j = 1, ..., M$. In this work, we employ a standard Monte Carlo sampling scheme, although sometimes there might be advantage in using other sampling methods.[40] The first-order functions are assumed to take the form of an expansion in orthogonal polynomials

$$A_i(k_i) = a_0 L_0(k_i) + a_1 L_1(k_i) + ... + a_m L_m(k_i) - \tau_0 \tag{2.9}$$

which are typically chosen to be (shifted) Legendre polynomials so that $\langle L_n \rangle = \delta_{0,n}$. The coefficients a_n are obtained by fitting τ to $A_i + \tau_0$ employing the full data set using linear regression.[41,42] The process is repeated using the same data set for each factor k_i. The second-order terms are found by a similar expansion

$$B_{i,j}(k_i, k_j) = \sum_{r=1}^{m_i} \sum_{s=1}^{m_j} b_{r,s} L_r(k_i) \, L_s(k_j) \tag{2.10}$$

The fitting can be carried out using the full first + second expansion, $\tau \approx \tau_0 + A_i + A_j + B_{i,j}$. Alternatively, the first-order component functions can be obtained separately, and the second-order function can be fit to the remainder $\tau - A_i - A_j - \tau_0$. Because there are $N(N - 1)/2$ distinct second-order expansions, we presume that a fitting for all pairs might not be feasible for a large mechanism. The order for the expansions in eqs 2.9 and 2.10 are set by trial and error (although see ref 41 for a discussion of the convergence properties with respect to the order of the fitting); overfitting is avoided if the A_i and $B_{i,j}$ values are expanded to seventh order or less. The overall fitting errors are expected to reflect the Monte Carlo sampling scheme and scale with $1/M^{1/2}$.

B. Combustion Modeling. The general outline of the mechanism improvement method was presented in the previous section. Now, we consider the specific adaptation of this method to the methanol combustion mechanism of Li et al.[23] The target selected is the ignition delay time, which is a numerically computed function. The autoignition of spatially homogeneous fuel/O_2 mixtures was simulated using the Chemkin II[43] suite of programs with the LSODE[44] integrator. The kinetic trajectories were integrated assuming a constant volume and thermally isolated reaction chamber. Thus, the equation governing the temperature is given by

$$\frac{\mathrm{d}T}{\mathrm{d}t} = -\frac{\dot{U}}{C_V} \tag{3.1}$$

where $\dot{U}$ is the rate of chemical generation of thermodynamic energy and C_V is the total heat capacity at constant volume. All species reside in the gas phase and are described by the ideal gas law. For all simulations, the initial concentrations of free radicals were assumed to be zero. As shown in Figure 2, the ignition of CH_3OH/O_2 mixtures is a quite abrupt single-stage process and is apparent in a variety of observables including temperature, pressure, and species concentration. For simplicity, we define τ as the time required for the sample to achieve a given value of the temperature, usually $T_{ignition} = 1800$ K. Although small numerical differences would accrue for other definitions of τ, they are not important because the ordering of the main effects is insensitive to these details.

In the mechanism of Li et al.,[23] there are 93 reversible reactions and 18 distinct chemical species used to model the chemistry. The kinetic mechanism and data employed are listed in Table 1. It is important to specify precisely how these rate coefficients are sampled when extracting the main effects. The bimolecular and termolecular rate coefficients are represented in the usual three-parameter form

$$k(T) = AT^{\delta} \mathrm{e}^{-E_a/k_B T} \tag{3.2}$$

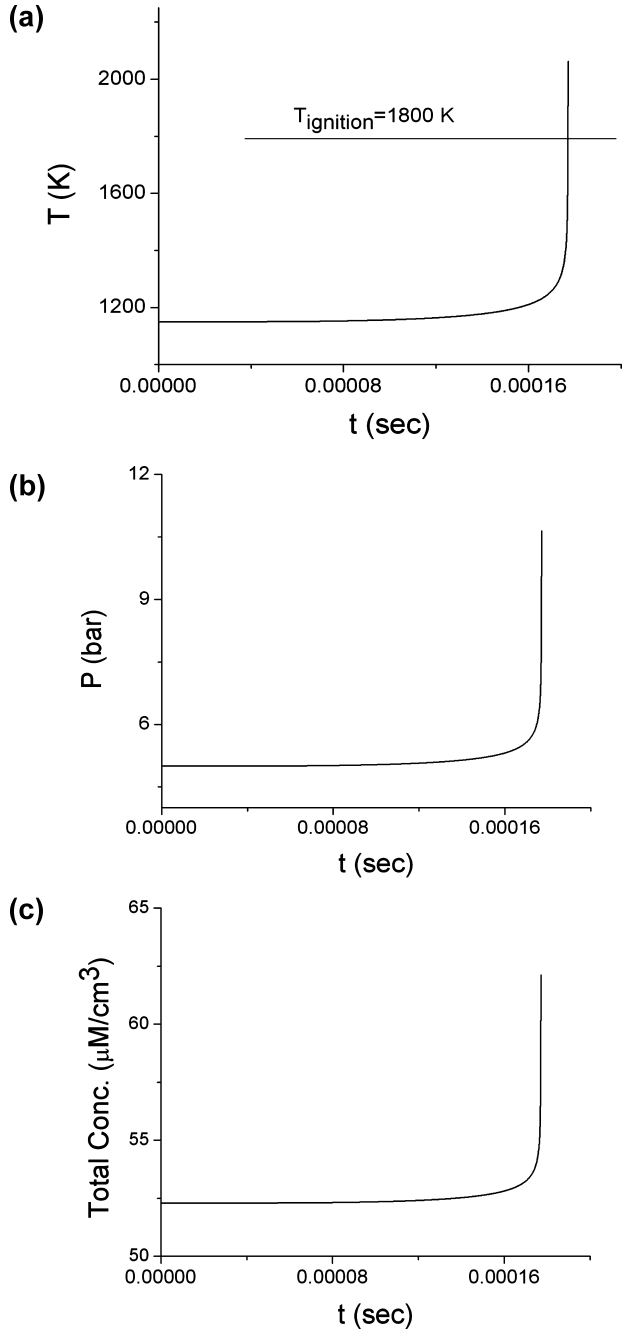

Figure 2. Ignition process represented in (a) temperature, (b) pressure, and (c) total species concentration versus time. The system exhibits a clear single-stage ignition near $t = 0.177$ ms. The conditions of the simulation are (T, P, Φ) = (1150 K, 5 bar, 1).

The pressure-dependent decomposition/recombination reactions are modeled using the Troe centering expression

$$k = k_\infty\left(\frac{P_r}{1+P_r}\right)F \tag{3.3}$$

with

$$P_r = \frac{k_0[\mathrm{M}]}{k_\infty} \tag{3.4}$$

where the high-pressure limit, k_∞, and the low-pressure limit, k_0, are each parametrized by distinct expressions of the form 3.2. The function F is given by Troe and co-workers.[45] The rate coefficients for the reverse reactions are defined in terms of the concentration equilibrium constant

$$k_r = \frac{k_f}{K_{eq}^c} \tag{3.5}$$

The use of eq 3.5 introduces additional empirical parameters into the model through the thermochemistry, which is discussed later. In principle, the response surface τ should be regarded as a function of all three fitting parameters (A, δ, E_a) for each rate coefficient. In practice, however, this would prove to be greatly redundant, especially given the lack of knowledge of the temperature dependence of the uncertainties of the rate coefficients. Variations in two of the parameters, (δ, E_a), effectively control the relative uncertainty of a given rate as a function of T. To screen the importance of a given reaction, it is sufficient to merely sample the pre-exponential factor A with the understanding that the relative importance of a reaction might change as a function of T. We note that such a temperature dependence of the main effects would occur even if all three parameters were screened because of the change in the underlying kinetics itself with T. The uncertainties of the rate constants reported in the literature are thus converted into uncertainties of the A factors

$$\Delta(\log k) \rightarrow \Delta(\log A) \tag{3.6}$$

If there were no uncertainty in the thermochemistry of the chemical species, the uncertainty ranges for the forward and reverse rate coefficients would be equal, and k_f would uniquely determine k_r through eq 3.5. However, if the heats of formation of the compounds in the mechanism are also regarded as uncertain factors, then the response surface becomes a function of $93 + 18 = 111$ parameters using

$$\log A_r = \log A_f - \Delta H_{rxn}^0/RT_0 \tag{3.7}$$

where ΔH_{rxn}^0 is composed from the appropriate sum of individual heats of formation and T_0 is the reference temperature used in the thermochemistry.

The distribution function for rate coefficients, $P(k)$, has until now been left unspecified. In this work,[46] we shall adopt the simple uniform distribution for a given k in the range (k_-, k_+)

$$P(k) = \frac{1}{k_+ - k_-} \quad k_\pm = k(|\Delta \log k|)^{\pm 1} \tag{3.8}$$

where the reported values for $\Delta(\log k)$ are assumed to be temperature-independent (see Table 1). The distribution 3.8 is generated by a standard Monte Carlo method, where a uniform random number between 0 and 1, x, is used to generate the pre-exponential factor through

$$A = A_- + x(A_+ - A_-) \tag{3.9}$$

where $A_\pm = A(|\Delta\log k|)^{\pm 1}$. In the present work, we cap the uncertainties in k at a factor of 5, although we shall see that

TABLE 1: Methanol Combustion Mechanism and Kinetic Data

species	ΔH_f^0 (kJ/mol)[a]
1. CH_3OH	0.18
2. O_2	0.167
3. CO	0.026
4. CO_2	0.014
5. CH_2O	0.46
6. H_2O	0.03
7. CH_4	0.3
8. H_2	0
9. H_2O_2	0.07
10. CH_3	0.1
11. H	0.000034
12. OH	0.04
13. CH_2OH	0.37
14. HCO	2.0
15. HO_2	0.58
16. O	0.1
17. CH_3O	0.42
18. C_2H_6	0.2

$k = AT^{\delta} \exp(-k_B T)^b$

	A	δ	E	$\lvert\Delta k/k\rvert$[60,61]
1. $H + O_2 = O + OH$	3.55×10^{15}	−0.4	16599.0	1.26
2. $O + H_2 = H + OH$	5.08×10^{4}	2.7	6290.0	3.16
3. $H_2 + OH = H_2O + H$	2.16×10^{8}	1.5	3430.0	2.0
4. $O + H_2O = OH + OH$	2.97×10^{6}	2.0	13400.0	2.5
5. $H_2 + M = H + H + M$	4.58×10^{19}	−1.4	104380.0	3.0
H_2	enhanced by	2.500×10^{0}		
H_2O	enhanced by	1.200×10^{1}		
CO	enhanced by	1.900×10^{0}		
CO_2	enhanced by	3.800×10^{0}		
Ar	enhanced by	0.000×10^{0}		
He	enhanced by	0.000×10^{0}		
6. $H_2 + AR = H + H + AR$	5.84×10^{18}	−1.1	104380.0	3.0
7. $H_2 + HE = H + H + HE$	5.84×10^{18}	−1.1	104380.0	3.0
8. $O + O + M = O_2 + M$	6.16×10^{15}	−0.5	0.0	2.0
H_2	enhanced by	2.500×10^{0}		
H_2O	enhanced by	1.200×10^{1}		
Ar	enhanced by	0.000×10^{0}		
He	enhanced by	0.000×10^{0}		
CO	enhanced by	1.900×10^{0}		
CO_2	enhanced by	3.800×10^{0}		
9. $O + O + AR = O_2 + Ar$	1.89×10^{13}	0.0	−1788.0	2.0
10. $O + O + HE = O_2 + He$	1.89×10^{13}	0.0	−1788.0	2.0
11. $O + H + M = OH + M$	4.71×10^{18}	−1.0	0.0	5.0
H_2	enhanced by	2.500×10^{0}		
H_2O	enhanced by	1.200×10^{1}		
Ar	enhanced by	7.500×10^{-1}		
He	enhanced by	7.500×10^{-1}		
CO	enhanced by	1.900×10^{0}		
CO_2	enhanced by	3.800×10^{0}		
12. $H + OH + M = H_2O + M$	3.80×10^{22}	−2.0	0.0	2.0
H_2	enhanced by	2.500×10^{0}		
H_2O	enhanced by	1.200×10^{1}		
Ar	enhanced by	3.800×10^{-1}		
He	enhanced by	3.800×10^{-1}		
CO	enhanced by	1.900×10^{0}		
CO_2	enhanced by	3.800×10^{0}		
13. $H + O_2 (+M) = HO_2 (+M)$	1.48×10^{12}	0.6	0.0	3.16
low-pressure limit:	0.63660×10^{21}	-0.17200×10^{1}	0.52480×10^{3}	
Troe centering:	0.80000×10^{0}	0.10000×10^{-29}	0.10000×10^{31}	
H_2	enhanced by	2.000×10^{0}		
H_2O	enhanced by	1.100×10^{1}		
O_2	enhanced by	7.800×10^{-1}		
CO	enhanced by	1.900×10^{0}		
CO_2	enhanced by	3.800×10^{0}		
14. $HO_2 + H = H_2 + O_2$	1.66×10^{13}	0.0	823.0	2.0
15. $HO_2 + H = OH + OH$	7.08×10^{13}	0.0	295.0	2.0
16. $HO_2 + O = O_2 + OH$	3.25×10^{13}	0.0	0.0	3.16
17. $HO_2 + OH = H_2O + O_2$	2.89×10^{13}	0.0	−497.0	3.16
18. $HO_2 + HO_2 = H_2O_2 + O_2$	4.20×10^{14}	0.0	11982.0	5.0
declared duplicate reaction...				

TABLE 1: Continued

	$k = AT^{\delta} \exp(-k_B T)^b$			
	A	δ	E	$\lvert\Delta k/k\rvert$[60,61]
19. $HO_2 + HO_2 = H_2O_2 + O_2$	1.30×10^{11}	0.0	−1629.3	5.0
declared duplicate reaction...				
20. H_2O_2 (+M) = OH + OH (+M)	2.95×10^{14}	0.0	48430.0	3.16
low-pressure limit:	0.12020×10^{18}	0.00000×10^{0}	0.45500×10^{5}	
Troe centering:	0.50000×10^{0}	0.10000×10^{-29}	0.10000×10^{31}	
H_2	enhanced by	2.500×10^{0}		
H_2O	enhanced by	1.200×10^{1}		
CO	enhanced by	1.900×10^{0}		
CO_2	enhanced by	3.800×10^{0}		
Ar	enhanced by	6.400×10^{-1}		
He	enhanced by	6.400×10^{-1}		
21. $H_2O_2 + H = H_2O + OH$	2.41×10^{13}	0.0	3970.0	5.0
22. $H_2O_2 + H = HO_2 + H_2$	4.82×10^{13}	0.0	7950.0	5.0
23. $H_2O_2 + O = OH + HO_2$	9.55×10^{6}	2.0	3970.0	3.0
24. $H_2O_2 + OH = HO_2 + H_2O$	1.00×10^{12}	0.0	0.0	1.26
declared duplicate reaction...				
25. $H_2O_2 + OH = HO_2 + H_2O$	5.80×10^{14}	0.0	9557.0	5.0
declared duplicate reaction...				
26. CO + O (+M) = CO_2 (+M)	1.80×10^{10}	0.0	2384.0	2.6
low-pressure limit:	0.15500×10^{25}	-0.27900×10^{1}	0.41910×10^{4}	
H_2	enhanced by	2.500×10^{0}		
H_2O	enhanced by	1.200×10^{1}		
AR	enhanced by	8.700×10^{-1}		
CO	enhanced by	1.900×10^{0}		
CO_2	enhanced by	3.800×10^{0}		
27. $CO + O_2 = CO_2 + O$	2.53×10^{12}	0.0	47700.0	2.0
28. $CO + HO_2 = CO_2 + OH$	3.01×10^{13}	0.0	23000.0	5.0
29. $CO + OH = CO_2 + H$	2.23×10^{5}	1.9	−1158.7	3.16
30. HCO + M = H + CO + M	4.75×10^{11}	0.7	14874.0	3.16
H_2	enhanced by	2.500×10^{0}		
H_2O	enhanced by	6.000×10^{0}		
CO	enhanced by	1.900×10^{0}		
CO_2	enhanced by	3.800×10^{0}		
31. $HCO + O_2 = CO + HO_2$	7.58×10^{12}	0.0	410.0	5.0
32. $HCO + H = CO + H_2$	7.23×10^{13}	0.0	0.0	2.0
33. HCO + O = CO + OH	3.02×10^{13}	0.0	0.0	2.0
34. HCO + OH = CO + H_2O	3.02×10^{13}	0.0	0.0	3.0
35. HCO + O = CO_2 + H	3.00×10^{13}	0.0	0.0	3.0
36. $HCO + HO_2 = CO_2 + OH + H$	3.00×10^{13}	0.0	0.0	5.0
37. $HCO + CH_3 = CO + CH_4$	1.20×10^{14}	0.0	0.0	2.0
38. HCO + HCO = H_2 + CO + CO	3.00×10^{12}	0.0	0.0	5.0
39. HCO + HCO = CH_2O + CO	3.00×10^{13}	0.0	0.0	2.0
40. $CH_2O + M = HCO + H + M$	3.30×10^{39}	−6.3	99900.0	3.16
H_2	enhanced by	2.500×10^{0}		
H_2O	enhanced by	1.200×10^{1}		
CO	enhanced by	1.900×10^{0}		
CO_2	enhanced by	3.800×10^{0}		
Ar	enhanced by	7.000×10^{-1}		
41. $CH_2O + M = CO + H_2 + M$	3.10×10^{45}	−8.0	97510.0	3.16
H_2	enhanced by	2.500×10^{0}		
H_2O	enhanced by	1.200×10^{1}		
CO	enhanced by	1.900×10^{0}		
CO_2	enhanced by	3.800×10^{0}		
AR	enhanced by	7.000×10^{-1}		
42. $CH_2O + H = HCO + H_2$	5.74×10^{7}	1.9	2748.6	2.0
43. $CH_2O + O = HCO + OH$	1.81×10^{13}	0.0	3080.0	2.0
44. $CH_2O + OH = HCO + H_2O$	3.43×10^{9}	1.2	−447.0	5.0
45. $CH_2O + O_2 = HCO + HO_2$	1.23×10^{6}	3.0	52000.0	3.16
46. $CH_2O + HO_2 = HCO + H_2O_2$	4.11×10^{4}	2.5	10210.0	3.16
47. $CH_2O + CH_3 = HCO + CH_4$	3.64×10^{-6}	5.4	998.0	2.0
48. $CH_3 + O = CH_2O + H$	8.43×10^{13}	0.0	0.0	1.58
49. $CH_3 + O_2 = CH_3O + O$	1.99×10^{18}	−1.6	29230.0	3.16
50. $CH_3 + O_2 = CH_2O + OH$	3.74×10^{11}	0.0	14640.0	5.0
51. $CH_3 + HO_2 = CH_3O + OH$	2.41×10^{10}	0.8	−2325.0	3.0
52. $CH_3 + CH_3$ (+M) = C_2H_6 (+M)	9.21×10^{16}	−1.2	635.8	2.0
low-pressure limit:	0.11350×10^{37}	-0.52460×10^{1}	0.17050×10^{4}	
Troe centering:	0.40500×10^{0}	0.11200×10^{4}	0.69600×10^{2}	0.10000×10^{16}
H_2	enhanced by	2.000×10^{0}		
H_2O	enhanced by	5.000×10^{0}		
CO	enhanced by	2.000×10^{0}		
CO_2	enhanced by	3.000×10^{0}		
53. CH_3 + H (+M) = CH_4 (+M)	1.27×10^{16}	−0.6	383.0	3.2
low-pressure limit:	0.24770×10^{34}	-0.47600×10^{1}	0.24400×10^{4}	
Troe centering:	0.78300×10^{0}	0.74000×10^{2}	0.29410×10^{4}	0.69640×10^{4}

TABLE 1: Continued

	$k = AT^{\delta}\exp(-k_BT)^b$			
	A	δ	E	$\lvert\Delta k/k\rvert^{60,61}$
H_2	enhanced by	2.000×10^0		
H_2O	enhanced by	6.000×10^0		
CH_4	enhanced by	2.000×10^0		
CO	enhanced by	1.500×10^0		
CO_2	enhanced by	2.000×10^0		
C_2H_6	enhanced by	3.000×10^0		
Ar	enhanced by	7.000×10^{-1}		
54. $CH_4 + H = CH_3 + H_2$	5.47×10^7	2.0	11210.0	1.58
55. $CH_4 + O = CH_3 + OH$	3.15×10^{12}	0.5	10290.0	2.0
56. $CH_4 + OH = CH_3 + H_2O$	5.72×10^6	2.0	2639.0	1.41
57. $CH_3 + HO_2 = CH_4 + O_2$	3.16×10^{12}	0.0	0.0	5.0
58. $CH_4 + HO_2 = CH_3 + H_2O_2$	1.81×10^{11}	0.0	18580.0	5.0
59. $CH_2OH + M = CH_2O + H + M$	1.00×10^{14}	0.0	25100.0	5.0
60. $CH_2OH + H = CH_2O + H_2$	6.00×10^{12}	0.0	0.0	2.0
61. $CH_2OH + H = CH_3 + OH$	9.64×10^{13}	0.0	0.0	2.0
62. $CH_2OH + O = CH_2O + OH$	4.20×10^{13}	0.0	0.0	2.0
63. $CH_2OH + OH = CH_2O + H_2O$	2.40×10^{13}	0.0	0.0	2.0
64. $CH_2OH + O_2 = CH_2O + HO_2$	2.41×10^{14}	0.0	5017.0	5.0
declared duplicate reaction...				
65. $CH_2OH + O_2 = CH_2O + HO_2$	1.51×10^{15}	−1.0	0.0	5.0
declared duplicate reaction...				
66. $CH_2OH + HO_2 = CH_2O + H_2O_2$	1.20×10^{13}	0.0	0.0	2.0
67. $CH_2OH + HCO = CH_3OH + CO$	1.00×10^{13}	0.0	0.0	5.0
68. $CH_2OH + HCO = CH_2O + CH_2O$	1.50×10^{13}	0.0	0.0	5.0
69. $2CH_2OH = CH_3OH + CH_2O$	3.00×10^{12}	0.0	0.0	2.0
70. $CH_2OH + CH_3O = CH_3OH + CH_2O$	2.40×10^{13}	0.0	0.0	2.0
71. $CH_3O + M = CH_2O + H + M$	8.30×10^{17}	−1.2	15500.0	2.0
72. $CH_3O + H = CH_3 + OH$	3.20×10^{13}	0.0	0.0	5.0
73. $CH_3O + O = CH_2O + OH$	6.00×10^{12}	0.0	0.0	5.0
74. $CH_3O + OH = CH_2O + H_2O$	1.80×10^{13}	0.0	0.0	5.0
75. $CH_3O + O_2 = CH_2O + HO_2$	9.03×10^{13}	0.0	11980.0	5.0
declared duplicate reaction...				
76. $CH_3O + O_2 = CH_2O + HO_2$	2.20×10^{10}	0.0	1748.0	5.0
declared duplicate reaction...				
77. $CH_3O + HO_2 = CH_2O + H_2O_2$	3.00×10^{11}	0.0	0.0	5.0
78. $CH_3O + CO = CH_3 + CO_2$	1.60×10^{13}	0.0	11800.0	5.0
79. $CH_3O + HCO = CH_3OH + CO$	9.00×10^{13}	0.0	0.0	3.0
80. $2CH_3O = CH_3OH + CH_2O$	6.00×10^{13}	0.0	0.0	5.0
81. $OH + CH_3$ (+M) ⇔ CH_3OH (+M)	2.79×10^{18}	−1.4	1330.0	2.0
low-pressure limit:	0.40000×10^{37}	-0.59200×10^1	0.31400×10^4	
Troe centering:	0.41200×10^0	0.19500×10^3	0.59000×10^4	0.63940×10^4
H_2	enhanced by	2.000×10^0		
H_2O	enhanced by	6.000×10^0		
CH_4	enhanced by	2.000×10^0		
CO	enhanced by	1.500×10^0		
CO_2	enhanced by	2.000×10^0		
C_2H_6	enhanced by	3.000×10^0		
82. $H + CH_2OH$ (+M) ⇔ CH_3OH (+M)	1.06×10^{12}	0.5	86.0	5.0
low-pressure limit:	0.43600×10^{32}	-0.46500×10^1	0.50800×10^4	
Troe centering:	0.60000×10^0	0.10000×10^3	0.90000×10^5	0.10000×10^5
H_2	enhanced by	2.000×10^0		
H_2O	enhanced by	6.000×10^0		
CH_4	enhanced by	2.000×10^0		
CO	enhanced by	1.500×10^0		
CO_2	enhanced by	2.000×10^0		
C_2H_6	enhanced by	3.000×10^0		
83. $H + CH_3O$ (+M) ⇔ CH_3OH (+M)	2.43×10^{12}	0.5	50.0	3.0
low-pressure limit:	0.46600×10^{42}	-0.74400×10^1	0.14080×10^5	
Troe centering:	0.70000×10^0	0.10000×10^3	0.90000×10^5	0.10000×10^5
H_2	enhanced by	2.000×10^0		
H_2O	enhanced by	6.000×10^0		
CH_4	enhanced by	2.000×10^0		
CO	enhanced by	1.500×10^0		
CO_2	enhanced by	2.000×10^0		
C_2H_6	enhanced by	3.000×10^0		
84. $CH_3OH + H = CH_2OH + H_2$	3.20×10^{13}	0.0	6095.0	5.0
85. $CH_3OH + H = CH_3O + H_2$	8.00×10^{12}	0.0	6095.0	5.0
86. $CH_3OH + O = CH_2OH + OH$	3.88×10^5	2.5	3080.0	5.0
87. $CH_3OH + OH = CH_3O + H_2O$	1.00×10^6	2.1	496.7	5.0
88. $CH_3OH + OH = CH_2OH + H_2O$	7.10×10^6	1.8	−596.0	5.0
89. $CH_3OH + O_2 = CH_2OH + HO_2$	2.05×10^{13}	0.0	44900.0	5.0
90. $CH_3OH + HCO = CH_2OH + CH_2O$	9.64×10^3	2.9	13110.0	5.0
91. $CH_3OH + HO_2 = CH_2OH + H_2O_2$	3.98×10^{13}	0.0	19400.0	5.0
92. $CH_3OH + CH_3 = CH_2OH + CH_4$	3.19×10^1	3.2	7172.0	3.0
93. $CH_3O + CH_3OH = CH_3OH + CH_2OH$	3.00×10^{11}	0.0	4060.0	5.0

[a] Uncertainty in heat of formation.[59] [b] Units of A are mol cm s K; units of E are cal/mol.

this is likely an underestimate of the true uncertainty. Several of the 93 reactions in the methanol mechanism are duplicates, that is, they have identical reagents and products to other reactions in the mechanism but different rate coefficients. The linear combination of the duplicate rate expressions permits the construction of more complicated temperature dependences than does a single term of the form of eq 3.2. In the global uncertainty analysis, the main effects for duplicate reactions are computed

as if they were independent parameters. The total main effect for a given reaction is the sum of the main effects of the duplicates. If a duplicated reaction is selected for improvement, the computed expression $k_{TST}(T)$ is fit to the linear combination of duplicated terms.

C. Theoretical Determination of Rate Coefficients. To discuss the particular procedures employed to improve the rate coefficients, it is necessary to anticipate the outcome of the screening analysis so that specific reactions can be considered. We shall find that reaction Rxn 91, $CH_3OH + HO_2$, and reaction Rxn 89, $CH_3OH + O_2$, are the most important factors in τ over a wide range of conditions for nondilute mixtures. A detailed description of the theoretical procedures employed in the present ab initio TST predictions for these two reactions was provided in ref 25. For completeness, we provide a brief review of this analysis.

Both the HO_2 and O_2 species react with methanol through direct H-atom abstractions at one of two sites

$$CH_3OH + HO_2 \rightarrow CH_2OH + H_2O_2 \quad \text{(Rxn 91)}$$

$$CH_3OH + HO_2 \rightarrow CH_2OH + H_2O_2 \quad \text{(Rxn 94)}$$

$$CH_3OH + O_2 \rightarrow CH_2OH\cdots HO_2 \rightarrow CH_2OH + HO_2 \quad \text{(Rxn 89)}$$

$$CH_3OH + O_2 \rightarrow CH_3O\cdots HO_2 \rightarrow CH_3O + HO_2 \quad \text{(Rxn 95)}$$

Reactions Rxn 94 and Rxn 95, which produce methoxy rather than hydroxymethyl, are not part of the original 93-reaction mechanism. They were considered here because these products are only moderately more endothermic (9.4 kcal/mol).

The potential energy surfaces for both reactions were studied at the CCSD(T)/CBS//CASPT2//cc-pVTZ level. This approach involves multireference second-order perturbation theory (CASPT2)[47,48] geometry optimization and rovibrational analyses employing Dunning's correlation-consistent polarized valence triple-ζ (cc-pVTZ) basis set.[49,50] More accurate energies are then obtained from CCSD(T)[51] (coupled-cluster) calculations at these CASPT2 geometries with the aug-cc-pVTZ and aug-cc-pVQZ basis sets, followed by an extrapolation to the complete-basis-set (CBS) limit.[52] The active spaces employed in the CASPT2 analysis and other details are provided in ref 25. All of the electronic structure calculations were done with the Molpro program package.[53]

The potential energy surfaces and stationary-point structures for these two reactions are illustrated in Figures 3 and 4. The CCSD(T)/CBS//CASPT2//cc-pVTZ zero-point-corrected barriers for reactions Rxn 91 and Rxn 94 are 15.3 and 21.2 kcal/mol, respectively. For the reaction of CH_3OH with O_2, the abstraction transition state lies lower in energy than the asymptotic product energies. In particular, the product energy for reaction Rxn 89 is 46.7 kcal/mol, whereas the barrier height is 42.5 kcal/mol. The calculations for reactions Rxn 91 and Rxn 94 indicate that the rate coefficient for reaction Rxn 95 should be significantly lower than that for reaction Rxn 89, and so, the former reaction was not explicitly considered.

The rate coefficients were obtained from conventional transition-state theory employing the rigid-rotor harmonic-oscillator (RRHO) energy assumptions for most degrees of freedom.[54] One-dimensional torsional corrections and asymmetric Eckart

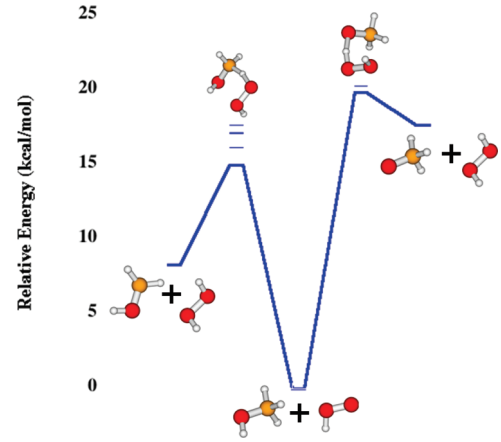

Figure 3. Transition-state structures and energy diagram for the reactions $CH_3OH + HO_2 = CH_2OH + H_2O_2$ and $CH_3OH + HO_2 = CH_3O + H_2O_2$ computed from ab initio quantum chemistry. The reaction barriers shown lie at 15.27 and 21.24 kcal/mol, including the zero-point corrections.

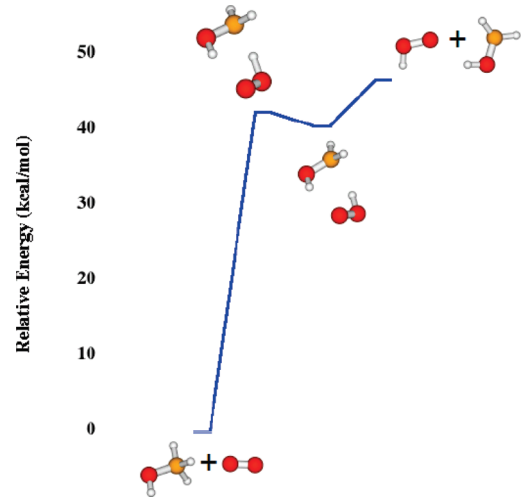

Figure 4. Transition-state structures and energy diagram for the $CH_3OH + O_2 = CH_2OH + HO_2$ reaction obtained from ab initio quantum chemistry. The reaction barriers shown are at 42.50 and 46.72 kcal/mol, including the zero-point corrections.

tunneling corrections were incorporated into the rate coefficient. For reaction Rxn 89, the abstraction bottleneck is followed by the formation of a van der Waals complex, with a second bottleneck to the formation of the bimolecular products. These two bottlenecks are considered to provide an effective flux arising from the two transition states acting in series. The flux for the decomposition of the van der Waals complex is treated with direct variable-reaction-coordinate transition-state theory (VRC-TST).[55−57]

The CCSD(T)/CBS predictions for the barrier heights are expected to be accurate to ~1.0 kcal/mol, which correlates to uncertainties of 1.65 and 1.28 at 1000 and 2000 K, respectively. Past experience suggests that similar magnitude uncertainties are expected from the TST and RRHO approximations, with these uncertainties expected to grow gradually with increasing temperature. Correspondingly, the overall predictions are expected to have an overall uncertainty of approimately a factor of 2 for the full range of temperatures of interest here (i.e., 800−2000 K).

III. Results

We now present the numerical results that characterize the mechanism improvement method for the methanol combustion

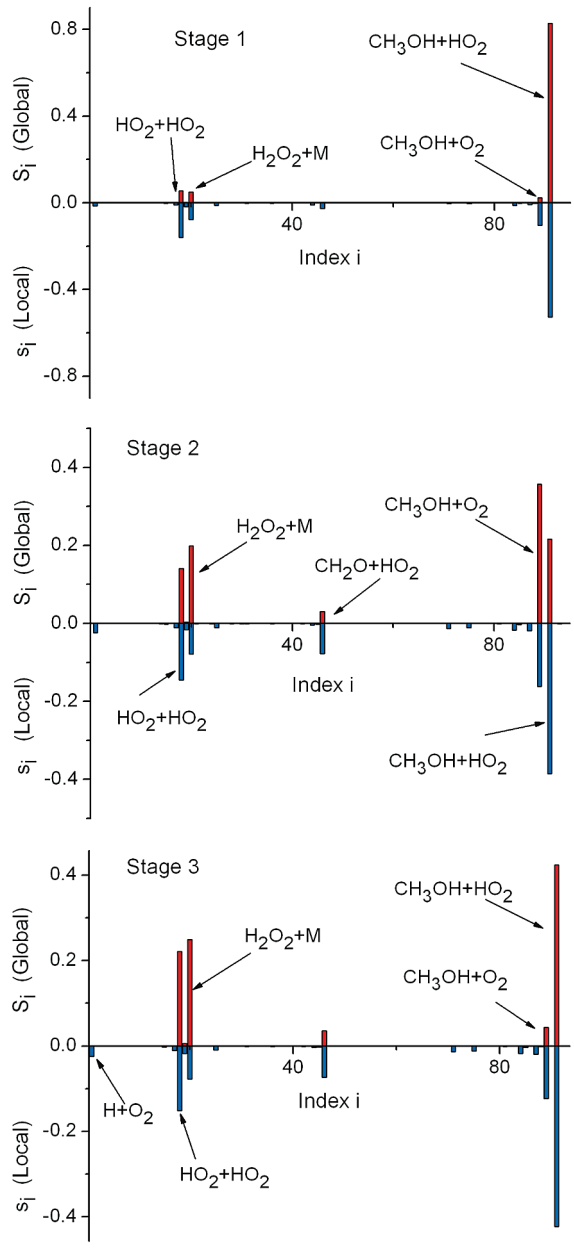

Figure 5. First-order global sensitivities, $S_i = \sigma_i^2/\sigma_T^2$, plotted versus the reaction index as red bars for stage 1, stage 2, and stage 3 mechanisms. The local sensitivities s_i (see eq 3.2) obtained under the same conditions are plotted with blue bars and are artificially made negative to aid visualization. The results are presented for $T = 1150$ K, $P = 5$ bar, and $\Phi = 1$, with no buffer gas present.

problem. We carry out the procedure described in the preceding section (steps 1−4) through two cycles of improvement. Although the resulting mechanism remains imperfect, we find that the overall uncertainty is systematically reduced.

The first step of our procedure is to apply the screening method to the original mechanism. The spectrum of sensitivity indices (i.e., S_i versus i) has been computed over a wide range of temperatures (T), pressures (P), and equivalence ratios (Φ). To illustrate the workings of the method, we consider in detail the case of $T = 1150$ K, $P = 5$ bar, and $\Phi = 1$. Using a uniform Monte Carlo distribution of $M = 20000$ points over the uncertainty ranges of the 93 rate coefficients, the spectrum of S_i obtained using the original mechanism of Li et al.[23] is shown in Figure 5. We refer to the original nominal mechanism as the stage 1 model. It is clear that the first-order variance is

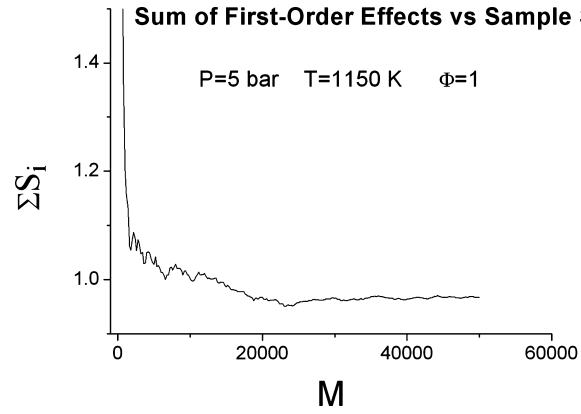

Figure 6. Sum of first-order sensitivity indices over all 93 factors as a function of the Monte Carlo sampling size for a simulation carried out under the conditions (T, P, Φ) = (1150 K, 5 bar, 1). The sum tends to about 0.98 at large M, indicating that the second- and higher-order sensitivities are relatively small.

dominated by just a few reactions that are labeled on the figure. The reaction $i = 91$, $CH_3OH + HO_2 = CH_2OH + H_2O_2$, is seen to dominate the global sensitivity, as it carries roughly 87% of the total variance of the response surface. For reference, we have also plotted in Figure 5 (as negative values) the local sensitivity coefficients obtained using eq 2.2 normalized to unity. There are important numerical differences between the local and global sensitivity analyses that, under some conditions, lead to different orderings of the relative importance of the reactions. In the present case, the local analysis correctly identifies reaction Rxn 91 as the most important, although it is not as quantitatively dominant as it is in the global analysis.

The convergence of the fitting procedure used to compute the component functions (and hence the partial variances) can be assessed by varying the sample size M. In Figure 6, we show the sum of the first-order sensitivity indices, $\sum S_i$, versus M. One can see that $\sum S_i$ apparently converges to about 0.98 for $M >$ 20000. Most of the "fitting error" in $\sum S_i$ at smaller values of M is the combined effect of a multitude of very small S_i values that are tending to (near) zero as $\sim 1/M^{1/2}$. The larger S_i values, which dominate the true variance, actually converge for much smaller values of M. Because $\sum S_i$ lies close to 1, the contributions to the variance of the higher-order sensitivities (i.e., interactions) are apparently quite small.

As we noted above, there is also a potential uncertainty in the mechanism through inaccuracies of the thermochemistry. To assess the importance of these effects, we also carried out additional computations including the literature uncertainties for the 18 distinct chemical species. It was found that, for all conditions of (T, P, Φ) considered, the contribution to the variance from the thermochemistry uncertainty was negligible compared to that from the rate coefficients. Indeed, the fractional contribution to the total variance of the thermochemistry terms was on the order of 0.1%. Hence, in what follows, we simply ignore the thermochemistry factors.

It is interesting to consider the behavior of the first-order component functions for the reactions that are selected as most important by our screening process. The reaction $CH_3OH + HO_2 = CH_2OH + H_2O_2$ (reaction $i = 91$) is clearly the dominant contributor to the variance in τ under the present conditions, constituting 87% of the variance. In Figure 7, we show ~1000 points from the data set in a scatter plot of τ vs x_{91} (recall that x_i goes between 0 and 1 over the uncertainty range of the ith reaction). We note that the data scattering seen in the figure is the result of random sampling of the other 93 − 1 = 92 rate

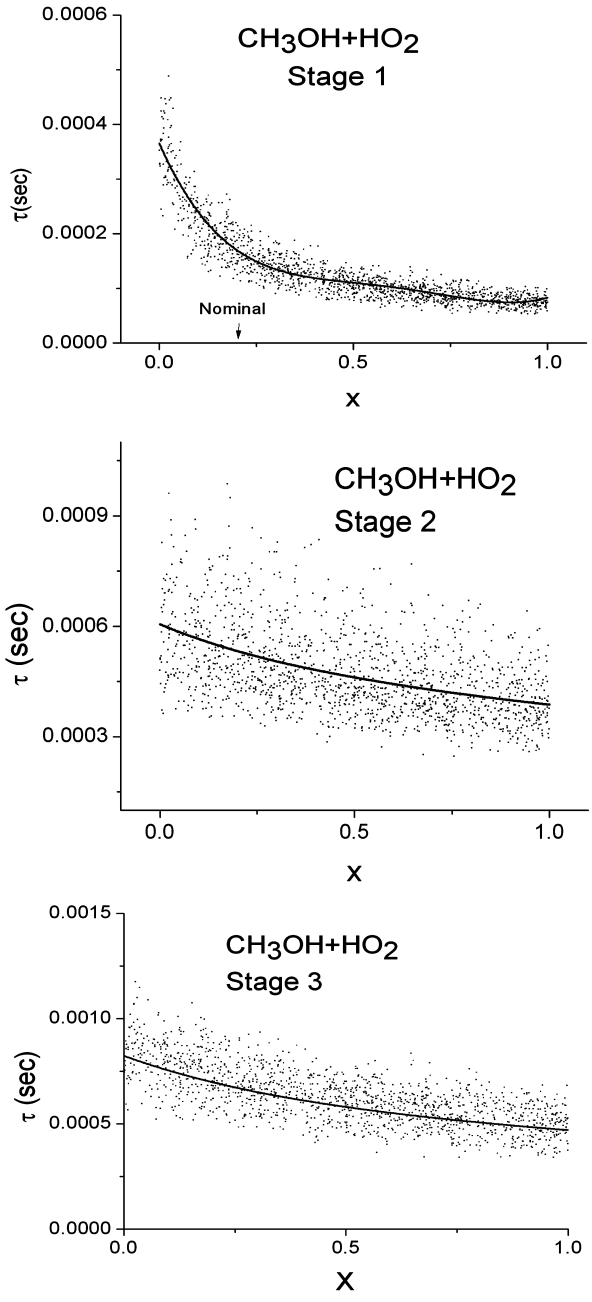

Figure 7. First-order component function for reaction Rxn 91 versus x for the three stages of the mechanism at (T, P, Φ) = (1150 K, 5 bar, 1). As defined in eq 3.9, x ranges from 0 to 1 over the uncertainty range of k. Also shown is a subset of the samples used in the fitting.

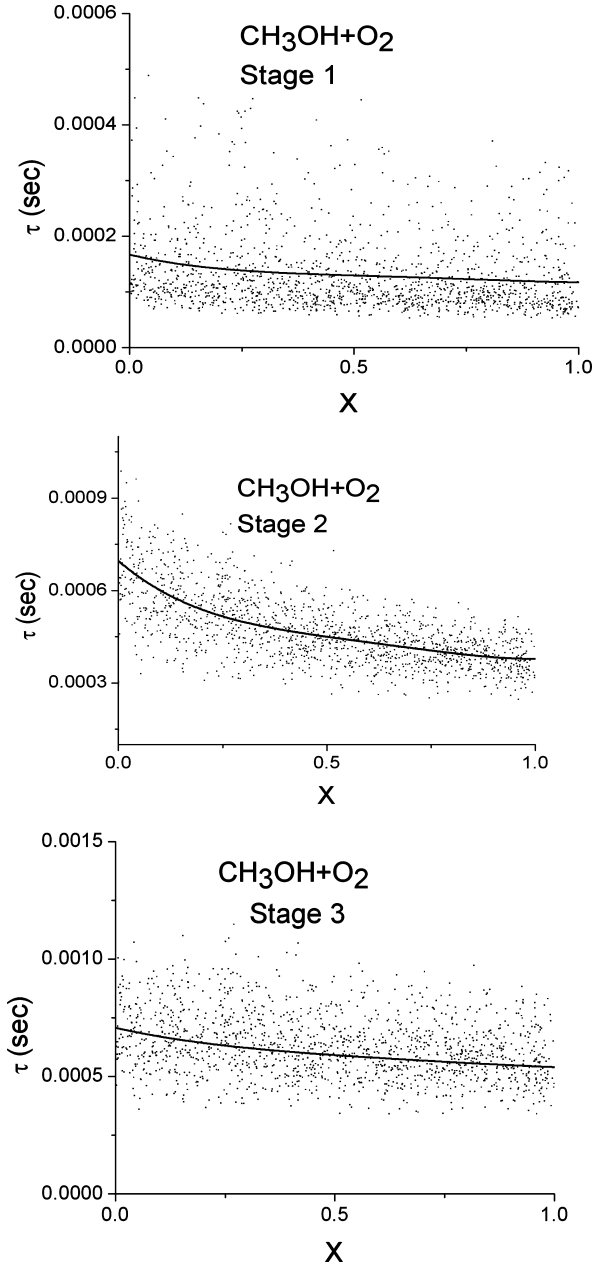

Figure 8. First-order component function for reaction Rxn 89 versus x for the three stages of the mechanism at (T, P, Φ) = (1150 K, 5 bar, 1). A subset of the Monte Carlo samples is also shown.

coefficients that are independent variables in τ. Any noise in the simulation due, for example, to integration error is much smaller than the data scatter in Figure 7. Shown with a solid line is the component function $A_{91}(x_{91}) + \tau_0$ computed using a fourth-order polynomial. Obviously, the ignition delay time shows a strong nonlinear correlation to the rate constant k_{91} not unlike that shown in Figure 1. For values of the rate constant lower than the nominal result of the Li et al.[23] mechanism, the response of τ is seen to be particularly strong. The analogous scatter plot and first-order component function for $CH_3OH + O_2 = CH_2OH + HO_2$ (reaction $i = 89$) at stage 1 is shown in Figure 8. It is seen that k_{89} has a much smaller influence on τ than did k_{91}, as the component function is relatively flat and shows only modest variation over the uncertainty range. We note that the spread of data points around the component function is much broader than it was for k_{91}, which emphasizes in a different way that τ is a relatively weak function of k_{89} at stage 1.

Although the higher-order component functions are clearly small for the present stage 1 model (because $\sum S_i = 0.98$ in first-order), we nevertheless computed some of the second-order terms to test the algorithm presented earlier. Because there are $92 \times 93/2 = 4278$ distinct second-order functions, we restrict our attention to the interactions that couple to one of the major reactions $i = 89$ or 91. It is reasonable to expect, although not strictly necessary, that the interactions to reactions that dominate in first order will be largest. In Figure 9, we show the second-order spectra, $S_{89,i} = \sigma_{89,i}^2/\sigma_T^2$ and $S_{91,i} = \sigma_{91,i}^2/\sigma_T^2$ computed using the data set of $M = 20000$. As might be expected, the level of statistical noise is higher than that for the first-order case as exhibiting the fluctuations in small terms in the spectra. The strongest interactions obtained were between reactions Rxn 91 and Rxn 89 and between reactions Rxn 91 and 18.

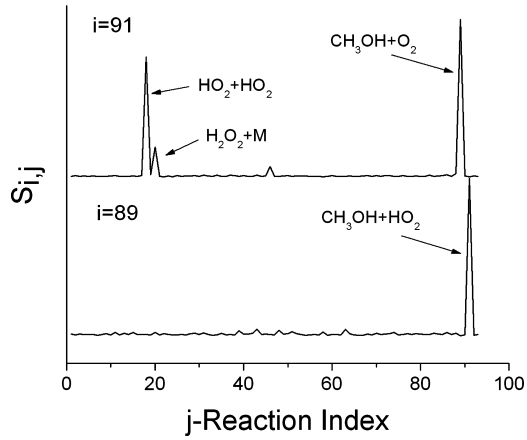

Figure 9. Second-order sensitivity indices $S_{91,j}$ and $S_{89,j}$ versus j for (T, P, Φ) = (1150 K, 5 bar, 1).

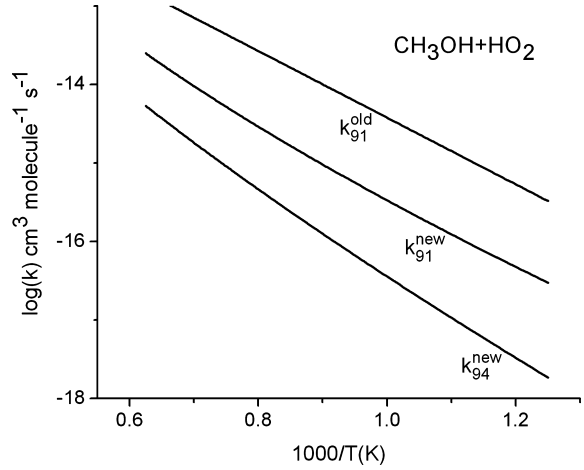

Figure 10. Rate coefficient for reaction Rxn 91, $CH_3OH + HO_2 \rightarrow CH_2OH + H_2O_2$, obtained from our theoretical computations (new) and the original results used by Li et al.[23] (old). Also shown is the much smaller rate coefficient for reaction Rxn 94, $CH_3OH + HO_2 \rightarrow CH_3O + H_2O_2$, obtained by us.

The next step in the mechanism improvement scheme is to update the rate coefficient for the reaction that has the highest sensitivity index S_i, namely, $CH_3OH + HO_2 = CH_2OH + H_2O_2$. The details of the quantum chemistry and TST calculations were presented in section II and in another publication,[25] and thus, we confine our discussion here to the points relevant to the kinetic modeling. First, we note that the investigation of the $CH_3OH + HO_2$ system actually reveals two transition states, one leading to the $CH_3O + H_2O_2$ products and the other leading to $CH_2OH + H_2O_2$. The first of these processes was not included in the original mechanism of Li et al.[23] Thus, at stage 2, the mechanism grows to 94 reversible steps with the inclusion of a new rate governed by k_{94}. However, because the rate coefficient for the new process is quite small, we find that it has a negligible influence on τ. In Figure 10, we show the rate coefficients versus temperature obtained from our theoretical computations, along with the values used in the model of Li et al.[23] The Arrhenius

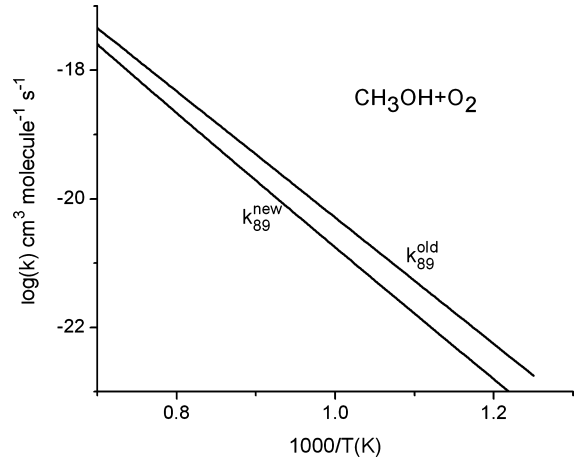

Figure 11. Rate coefficient for reaction Rxn 89, $CH_3OH + O_2 \rightarrow CH_2OH + HO_2$, obtained from our theoretical computations (new) and the original results used by Li et al.[23] (old).

parameters were obtained by numerical fitting and are presented in Table 2. We also point out that the rate coefficient for $CH_3OH + HO_2 \rightarrow CH_2OH + H_2O_2$ at 1150 K is 8.1 times smaller than in the original mechanism and thus lies in the highly nonlinear response regime seen in the upper panel of Figure 7. Clearly, we expect the ignition delay time to be longer at stage 2 than at stage 1. To continue with the refinement of the mechanism, we also require a new estimate for the uncertainty range of k, which was $\Delta k_{91}/k_{91} = 5$ for the original mechanism. The uncertainty range is a difficult quantity to define rigorously and is most often set by "expert opinion" based on a survey of the available literature. For the present theoretical determination of the rate coefficient, errors can accrue through inaccuracies in the computed potential surface and dynamical inaccuracies in the transition-state approximation. Our experience leads us to conclude that the errors in the present high-level calculations are fairly small and yield an uncertainty range of a factor of 2, that is, $\Delta\log(A_{91}) = \Delta\log(A_{94}) = 0.3$.

The new rate coefficients and uncertainty ranges are inserted into the screening method, which yields the stage 2 sensitivity spectrum shown in Figure 5. It is seen that $CH_3OH + HO_2$ is no longer the dominant contributor to the variance. Instead, the $CH_3OH + O_2 = CH_2OH + HO_2$ reaction ($i = 89$) is the largest, and the $HO_2 + HO_2 = H_2O_2 + O_2$ ($i = 20$) process has also grown more significant. We note that the main reason that S_i has become smaller for $i = 91$ is that the uncertainty range has been lowered. The first-order component functions for $i = 89$ and $i = 91$ are shown along with the scatter plot of data in Figures 7 and 8. It is seen that the component function for $i = 91$ is much flatter than it was at stage 1. On the other hand, the $i = 89$ component function shows much more variation than it did at stage 1.

The next level of mechanism improvement is achieved by updating the rate coefficient for the $CH_3OH + O_2 \rightarrow CH_2OH + HO_2$ reaction. In Figure 11, we show the rate coefficients versus temperature obtained from our theoretical computations, along with the values used in the model of Li et al.[23] Again,

TABLE 2: Arrhenius Parameters for Rate Coefficients: $k(T) = AT^{\delta}e^{-T_0/T}$

reaction	A (cm^3 s^{-1} molecule^{-1})	δ	T_0 (K)
$CH_3OH + HO_2 \rightarrow CH_2OH + H_2O_2$	3.78×10^{-29}	5.06	5140
$CH_3OH + HO_2 \rightarrow CH_3O + H_2O_2$	5.54×10^{-26}	4.12	8170
$CH_3OH + O_2 \rightarrow CH_2OH + HO_2$	5.95×10^{-19}	2.27	21520

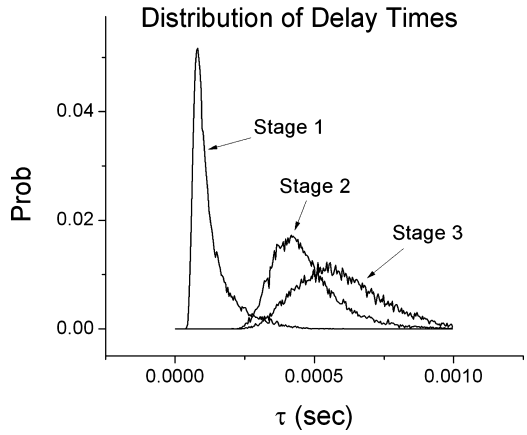

Figure 12. Probability distribution function (PDF) of ignition delay times obtained from the Monte Carlo sampling of the uncertainty hypervolume at (T, P, Φ) = (1150 K, 5 bar, 1). The mean of the distribution progressively grows as the model is refined, as does the apparent width of the distribution.

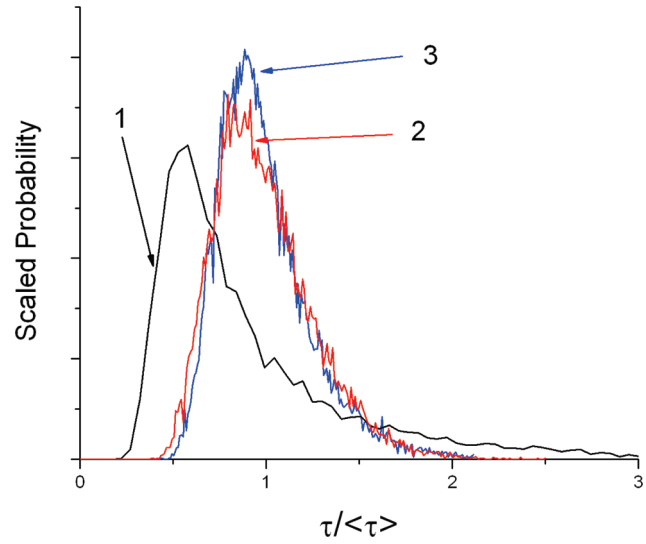

Figure 13. PDF of delay times shown in Figure 8 plotted in terms of the reduced variable $\tau/\langle\tau\rangle$.

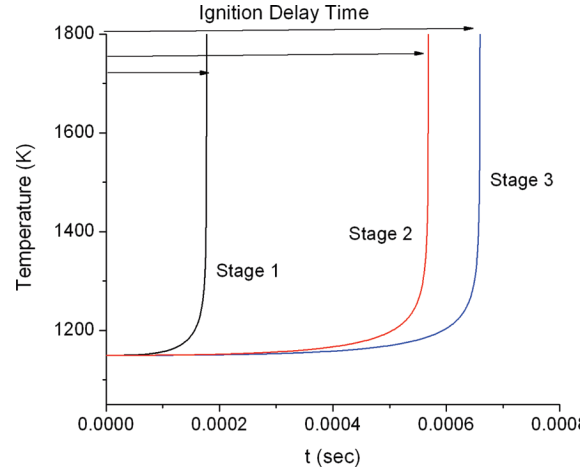

Figure 14. Ignition profiles for a mixture with (T, P, Φ) = (1150 K,5 bar,1) using the mechanisms at stages 1, 2, and 3.

the Arrhenius parameters were obtained by numerical fitting and are presented in Table 2. The new rate coefficient is found to be a factor of 5.8 times smaller than that in the original mechanism at T = 1150 K. Again, our experience with high-level theoretical computation of rate coefficients leads us to conclude that the uncertainty range will shrink to about a factor of 2 from the original factor of 5. The spectrum of sensitivity indices at stage 3 is shown in the lower panel of Figure 5. The contribution from the $CH_3OH + O_2 = CH_2OH + HO_2$ reaction is seen to fall dramatically, whereas reaction Rxn 91 grows to again be the largest contributor to the variance. Because reaction Rxn 91 has already been improved as much as possible at the present level of theory, further refinement of the mechanism should then move to the next-most-sensitive reaction, namely, the hydroperoxyl self-reaction $HO_2 + HO_2 = H_2O_2 + O_2$. For the present work, we are content to remain at the stage 3 model. The component functions, shown in Figures 7 and 8 for i = 89 and i = 91, respectively, exhibit a modest variation over the uncertainty ranges.

We now consider how the total uncertainty in the ignition delay time evolves as the mechanism is refined through stages. In Figure 12, we show the distribution functions of τ values obtained from the Monte Carlo sampling of the uncertainty hypercube at the three stages of modeling. Clearly, the mean value of τ, $\langle\tau\rangle$, becomes progressively larger as the model is refined. In absolute terms, the width of the distribution, $\Delta\tau$, appears to actually grow larger at later stages, suggesting that the overall uncertainty is growing even though the uncertainty ranges of the rate coefficients are shrinking. This seeming paradox is resolved if the distribution is plotted as a function of τ scaled to the mean (i.e., $\tau/\langle\tau\rangle$), as in Figure 13. In these dimensionless units, the width of the distribution decreases as the model is refined: $\Delta\tau/\langle\tau\rangle$ = 0.576, 0.284, and 0.266 at stages 1, 2, and 3, respectively. Although the relative error does decline as the mechanism is refined, it is important to realize that significant uncertainty in τ remains even at stage 3. Finally, in Figure 14, we show the ignition profiles for the stage 1, 2, and 3 mechanisms. Consistent with the evolution of the probability distribution functions, the ignition time increases by about a factor of 4 because of the updating of the rate coefficients. It is clear that the model improvement scheme employed here has had a major effect on the performance of the methanol combustion mechanism under these nondilute conditions.

Although we have focused thus far on mechanism improvement for the specific conditions (T, P, Φ) = (1150 K, 5 bar, 1), it is important to realize that the value of the sensitivity indices, and even their ordering, might depend on these choices. Therefore, to assess whether $CH_3OH + HO_2 = CH_2OH + H_2O_2$ and $CH_3OH + O_2 = CH_2OH + HO_2$ will continue to dominate the global sensitivity indices under other conditions, we carried out simulations for a range of combinations of (T, P, Φ). In Figures 15 and 16, we show three-dimensional plots of S_i versus (i, T) and (i, P), respectively, for Φ = 1 for the nominal mechanism of Li et al.[23] Although there are clearly quantitative effects of changing (T, P), under most conditions, we find that reaction Rxn 91, $CH_3OH + HO_2 = CH_2OH + H_2O_2$, continues to dominate the uncertainty spectrum. In Figure 15, for example, we see that this reaction yields $S_i \approx 0.87$ over the entire temperature range from 900 to 1600 K. Reaction Rxn 89, $CH_3OH + O_2$, grows significantly with T, whereas reaction 18, $HO_2 + HO_2$, falls off with T, although both remain secondary to reaction Rxn 91. There is a somewhat larger effect of pressure, which is shown in Figure 16. One can see that S_{91} falls off from 0.91 to 0.78 over the pressure range from 0.2 to 80 bar at T = 1150 K and Φ = 1. Over this pressure range, reactions 18 and 20 interchange as the second-most-important reaction. As we see next, however, there can be a much more profound effect on S_i for dilute mixtures.

Because the mechanism of Li et al.[23] was originally validated by comparison to experimental results, it is important to consider

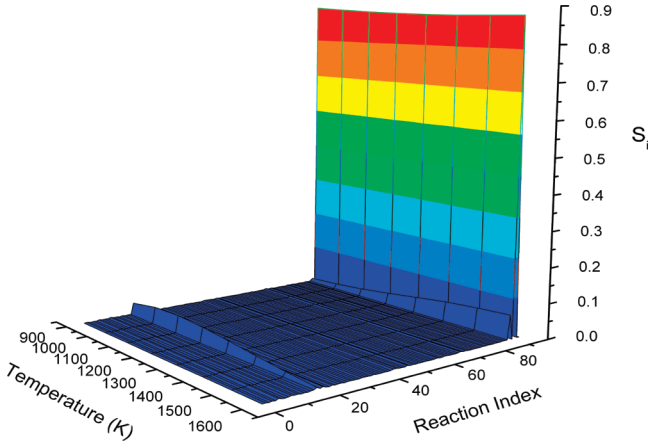

Figure 15. Spectrum of first-order sensitivity indices versus index and temperature at a fixed pressure of 5 bar and a fixed equivalence ratio of 1.

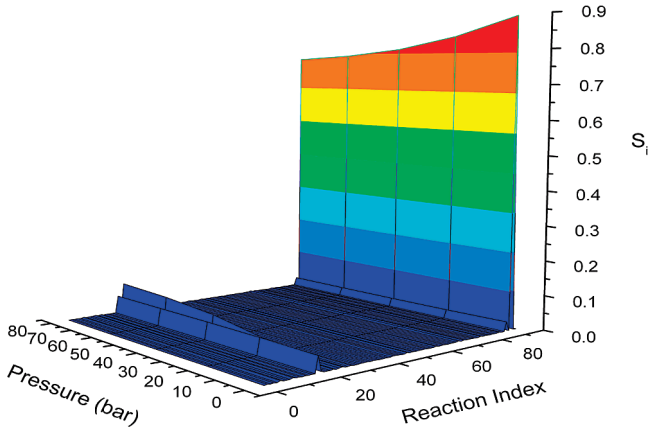

Figure 16. Spectrum of first-order sensitivity indices versus index and pressure at a fixed temperature of 1150 K and a fixed equivalence ratio of 1.

how the present modifications might affect the agreement with experiment. The ignition delay time for methanol/oxygen mixtures was measured by Bowman[58] using a shock tube technique for elevated temperatures, $T = 1545-2180$ K, under dilute conditions in an argon buffer, $P_{methanol} = 0.005-0.04$ bar, but with high total pressures $P > 1.5$ bar. In Figure 17, we show the results for the most highly concentrated conditions discussed by Li et al.,[23] mixture 1, which is still quite dilute although rich, $\Phi = 3$. In the upper panel, we show the delay time versus $1/T$ for the stage 1, 2, and 3 mechanisms, along with the experimental results. It is seen that updating the rate coefficients has a fairly small effect on τ in the experimental validation region. The stage 2 and 3 mechanisms appear to be a slight improvement on the original, which had tended to underestimate the value of τ. We note that, at lower temperatures, for which experiments are not available, the influence of the updates is much larger. Furthermore, as illustrated by the lower panel in Figure 17, the delay time can be increased by up to a factor of 8 as a result of being updated at low temperatures and high concentrations in the absence of a buffer.

It is apparent that the key reaction steps in the dilute-mixture/high-temperature regime must be different from those steps identified at high concentration/low temperature (i.e., reactions Rxn 91 and Rxn 89). Indeed, as was already noted by Li et al.,[23] a local sensitivity analysis at a set of experimental conditions (mixture 2) suggests that reaction 1, $H + O_2 = OH + O$, has the largest effect on the ignition delay time. In Figure 18, we show a comparison of the local and global sensitivity indices computed for the sample denoted as mixture 3. It can be seen that reactions Rxn 91 and Rxn 89 no longer dominate the variance in either the local or global treatments. Furthermore, the global sensitivity analysis gives a very different importance ordering of the reaction steps than does the local analysis. Whereas $H + O_2$ has the largest local sensitivity, $CH_3OH + H = CH_2OH + H_2$ (reaction 84) has the largest global index, with S_{84} being 3 times larger than S_1. The reactions $CH_2O + OH$ (reaction 44) and $OH + HO_2$ (reaction 17) likewise were found to be more important than reaction 1 in the global analysis.

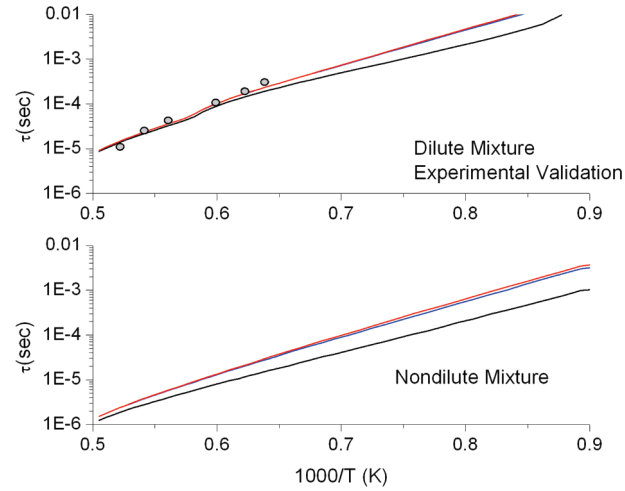

Figure 17. (Top) Predictions of models at stages 1, 2, and 3 (black, red, and blue, respectively) for the dilute conditions required for experimental validation (4% methanol, 2% oxygen, 94% argon, and thus $\Phi = 3$) at a total pressure of 1.5 bar. The experimental data, shown with symbols, were adjusted slightly to reflect the present definition of the ignition time. In the lower panel, results are shown for a high-concentration mixture (40% methanol, 60% oxygen, 0% argon, and hence $\Phi = 1$) again at 1.5 bar of total pressure.

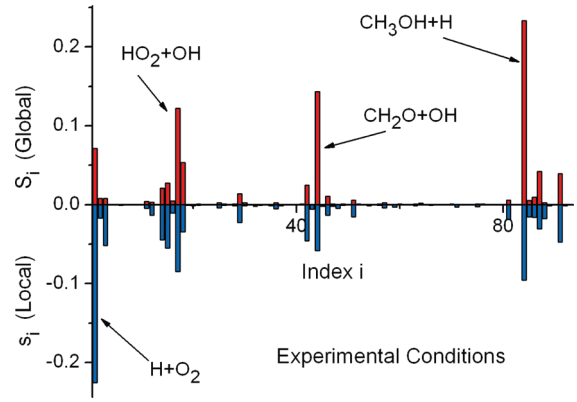

Figure 18. Global (red) and local (blue) sensitivity coefficients versus reaction index for the experimental validation conditions of $T = 1660$ K, $P = 4.3$ bar, 0.75% methanol, 1.5% oxygen, and 97.25% argon. This mixture corresponds to an equivalence ratio of $\Phi = 0.75$.

IV. Discussion and Conclusions

Chemical mechanisms are constantly being updated as new experiments and calculations yield improved kinetic data. In the present work, we have put forth a systematic method that is designed to improve a mechanism as gauged through the prediction of specific target functions. The approach is purely theoretical in that the rate coefficients are obtained using high-level quantum chemistry and transition-state theory calculations. Because the recalculation of all of the rate coefficients of a large

mechanism is not practical, a crucial element of our method is the use of a global sensitivity measure to identify the key reaction steps that require updating. Such a procedure is necessary to incorporate both the importance of a given rate coefficient in the target and the uncertainty of our knowledge of it. The present study of methanol combustion has emphasized several important points about the global sensitivity analysis. First, even though the mechanism might consist of many steps, the bulk of the variation of the target function can be controlled by just a few (or even one) uncertain rate constants. Indeed, we observed that k_{91} for the $CH_3OH + HO_2$ reaction was found to contribute roughly 90% of the variance in τ over a broad range of conditions for the stage 1 mechanism. Second, we found that importance ordering of the key reaction steps depended on the conditions of the simulation. Variation in the starting temperature, pressure, equivalence ratio, and pressure of buffer gases can have a major effect on the identification of key reactions. We observed that reactions Rxn 91 and Rxn 89 were most important under high-concentration "engine" conditions, whereas reactions 84, 44, and 17 carried the most variance under low-concentration "shock tube" conditions. Third, although an updated mechanism with an improved value for a rate coefficient must be regarded as superior to the original, it does not follow that the uncertainty of the target function must necessarily decrease. As seen in the present case, if a given sensitive rate coefficient is significantly altered, the uncertainty from the remaining $N - 1$ k_i values can be a strong function of the new value.

Finally, it is of interest to briefly consider the underlying chemistry that is responsible for the sensitivity of the ignition delay time to the various rate coefficients. The ignition process is heralded by the explosive growth in free-radical concentration brought on by chain-branching steps in the mechanism. For high-temperature/dilute conditions, the chain-branching reaction $H + O_2 = OH + O$ dominates the reactive flux and is often found to be the most critical step in determining the ignition delay time.[24] Because this reaction is very well studied and, hence, the uncertainty in k is small, we find other steps to be more important to update, such as $CH_3OH + H = CH_2OH + H_2$. This step involves the reaction of the dominant radical with the fuel molecule to create a fuel radical + H_2. It is the key chain-propagation step for the fuel and contributes to the radical pool through the formation of HO_2 in the reaction of the hydroxymethyl radical with oxygen and through the formation of H atoms in the decomposition of CH_2OH. Under low-temperature/high-concentration conditions, our analysis strongly identified $CH_3OH + HO_2 = CH_2OH + H_2O_2$ as the key step requiring updating. This reaction again involves a key chain-propagation step for the fuel where the reaction of the dominant radical (under these conditions) with the fuel molecule creates a fuel radical + closed-shell species. Perhaps more importantly, in this case, the H_2O_2 species is cogenerated, and H_2O_2 is known[24] to be intimately connected to ignition at lower temperatures through the chain-branching decomposition process $H_2O_2 + M \rightarrow 2OH + M$. The second-most-important reaction, $CH_3OH + O_2 \rightarrow CH_2OH + HO_2$, also converts the fuel to a radical while generating HO_2, which again reacts to form H_2O_2.

Acknowledgment. This work was supported by the Division of Chemical Sciences, Geosciences, and Biosciences, Office of Basic Energy Sciences, U.S. Department of Energy, under Contract DE-AC02-06CH11357. We are grateful to Dingyu Zhou for assistance on the manuscript.

References and Notes

(1) Westbrook, C. K.; Mizobuchi, Y.; Poinsot, T. J.; Smith, P. J.; Warnatz, J. *Proc. Combust. Inst.* **2005**, *30*, 125.
(2) Curran, H. J.; Gaffuri, P.; Pitz, W. J.; Westbrook, C. K. *Combust. Flame* **1998**, *114*, 149. Curran, H. J.; Gaffuri, P.; Pitz, W. J.; Westbrook, C. K. *Combust. Flame* **2002**, *129*, 253.
(3) Cohen, N. J. *J. Phys. Chem.* **1992**, *96*, 9052.
(4) Frenklach, M.; Wang, H.; Rabinowitz, M. J. *Prog. Energy Combust. Sci.* **1992**, *18*, 47.
(5) Eiteneer, B.; Yu, C.-L.; Goldenberg, M.; Frenklach, M. *J. Phys. Chem. A* **1998**, *102*, 5196.
(6) Frenklach, M.; Packard, A.; Seiler, P.; Feeley, R. *Int. J. Chem. Kinet.* **2004**, *36*, 57. Freeley, R.; Seiler, P.; Packard, A.; Frenklach, M. *J. Phys. Chem. A* **2004**, *108*, 9573.
(7) Welch, W. J.; Buck, R. J.; Sacks, J.; Wynn, H. P.; Mitchell, T. J.; Morris, M. D. *Technometrics* **1992**, *34*, 15.
(8) Cukier, R I.; Fortuin, C. M.; Schuler, K. E.; Petschet, A. G.; Schaiby, J. H. *J. Chem. Phys.* **1973**, *59*, 3873; *J. Chem. Phys.* **1973**, *59*, 3879.
(9) Zador, J.; Zsely, I. G.; Zador, I.; Turanyi, T. *Reliab. Eng. Syst. Saf.* **2006**, *91*, 1232.
(10) Cukier, R. I.; Levine, H. B.; Shuler, K. E. *J. Comput. Phys.* **1978**, *26*, 1.
(11) McRae, G. J.; Tilden, J. W.; Seinfeld, J. H. *Comput. Chem. Eng.* **1982**, *6*, 15.
(12) Miller, D.; Frenklach, M. *Int. J. Chem. Kin.* **1983**, *15*, 677.
(13) Rabitz, H.; Alis, O. F.; Shorter, J.; Shim, K. *Comput. Phys. Commun.* **1999**, *117*, 11.
(14) Rabitz, H. *J. Math. Chem.* **1999**, *25*, 197.
(15) Ziehn, T.; Tomlin, A. S. *Int. J. Chem. Kinet.* **2008**, *40*, 742.
(16) Zsely, I. G.; Zador, J.; Turanyi, T. *Int. J. Chem. Kinet.* **2009**, *40*, 754.
(17) Ziehn, T.; Tomlin, A. S. *Env. Model. Soft.* **2009**, *24*, 775.
(18) Ziehn, T.; Hughes, K. J.; Griffiths, J. F.; Porter, R.; Tomlin, A. S. *Combust. Theory Mod.* **2009**, *13*, 589.
(19) Russi, T.; Packard, A.; Feeley, R.; Frenklach, M. *J. Phys. Chem. A* **2008**, *112*, 2579.
(20) Saltelli, A. Chan, K., Scott, E. M. *Sensitivity Analysis*; John Wiley & Sons: Chichester, U.K., 2000.
(21) Ziehn, T. Ph.D. Thesis, The University of Leeds, Leeds, U.K., 2008.
(22) Agarwal, A. K. *Prog. Energy Combust. Sci.* **2007**, *33*, 233.
(23) Li, J.; Zhao, Z.; Kazakov, A.; Chaos, M.; Dryer, F. L.; Scire, J. J., Jr. *Int. J. Chem. Kinet.* **2007**, *39*, 109.
(24) Westbrook, C. K. *Proc. Combust. Inst.* **2000**, *28*, 1563.
(25) Klippenstein, S. J.; Harding, L. B.; Davis, M. J.; Tomlin, A. S.; Skodje, R. T. *Proc. Combust. Inst.*, manuscript accepted.
(26) Davis, M. J.; Tomlin, A. S.; Skodje, R. T., to be published.
(27) Zhou, D. Y.; Davis, M. J.; Skodje, R. T., to be published.
(28) Saltelli, A.; Ratto, M.; Andres, T.; Campolongo, F.; Cariboni, J.; Gatelli, D.; Sasana, M.; Tarantola, S. *Global Sensitivity Analysis. The Primer*; John Wiley & Sons: New York, 2008.
(29) Truhlar, D. G.; Garrett, B. C. *Acc. Chem. Res.* **1980**, *13*, 440.
(30) Miller, W. H.; Handy, N. C.; Adams, J. E. *J. Chem. Phys.* **1980**, *72*, 99.
(31) Skodje, R. T.; Truhlar, D. G.; Garrett, B. C. *J. Chem. Phys.* **1982**, *77*, 5955.
(32) Rabitz, H.; Kramer, M.; Dacol, D. *Annu. Rev. Phys. Chem.* **1983**, *34*, 419.
(33) Turanyi, T. *J. Math. Chem.* **1990**, *5*, 203.
(34) Scire, J. J., Jr.; Dryer, F. L.; Yetter, R. A. *Int. J. Chem. Kinet.* **2001**, *33*, 784.
(35) Morris, M. D. *Technometrics* **1991**, *33*, 161.
(36) Sobol, I. M. *Math. Comput. Simul.* **2001**, *55*, 271.
(37) Li, G.; Rosenthal, C.; Rabitz, H. *J. Phys. Chem. A* **2001**, *105*, 7765.
(38) Li, G.; Wang, S.-W.; Rabitz, H. *J. Phys. Chem. A* **2002**, *106*, 8721.
(39) Li, G.; Rabitz, H.; Yelvington, P.; Oluwole, O.; Bacon, F.; Kolb, C.; Schoendorf, J. *J. Phys. Chem. A* **2010**, *114*, 6022.
(40) Helton, J. C.; Johnson, J. D.; Sallaberry, C. J.; Storlie, C. B. *Reliab. Eng. Syst. Saf.* **2008**, *91*, 1175.
(41) Lewandowski, D.; Cooke, R. M.; Tebbens, R. J. D. *ACM Trans. Model. Comput. Simul.* **2007**, *18* (1), article 3.
(42) Mara, T. A.; Joseph, O. R. *J. Stat. Comput. Simul.* **2008**, *78*, 167.
(43) Kee, R. J.; Rupley, F.; Miller, J. A. *Chemkin II: A Fortran Chemical Kinetics Package for the Analysis of Gas-Phase Chemical Kinetics*; Report SAND-89-8009; Sandia National Laboratories: Albuquerque, NM, 1990.
(44) Radhakrishnan, K., Hindmarsh, A. C. *Description and Use of LSODE, the Livermore Solver for Ordinary Differential Equations*; LLNL Report UCRL-ID-113855; Lawrence Livermore National Laboratory: Livermore, CA, 1993.

(45) Gilbert, R. G.; Luther, K.; Troe, J. *Ber. Bunsen-Ges. Phys. Chem.* **1983**, *87*, 169. We define $\log F = \left\{1 + \left[\log P_r + c/n - d(\log P_r + c)\right]^2\right\}^{-1} \log F_{cent}$, where $F_{cent} = (1 - \alpha) \exp(-T/T^{***}) + \alpha \exp(T/T^{*}) + \exp(-T^{**}/T)$.

(46) In ref 25, we employed a somewhat different sampling scheme in which log(*A*) was uniformly weighted over the uncertainty range. Although slightly different numerical values were obtained for the sensitivity coefficients, the importance ordering of the reactions remained the same.

(47) Andersson, K.; Malmqvist, P.-A.; Roos, B. O. *J. Chem. Phys.* **1992**, *96*, 1218.

(48) Werner, H. -J. *Mol. Phys.* **1996**, *89*, 645. Celani, P.; Werner, H. -J. *J. Chem. Phys.* **2000**, *112*, 5546.

(49) Dunning, T. H., Jr. *J. Chem. Phys.* **1989**, *90*, 1007.

(50) Kendall, R. A.; Dunning, T. H., Jr.; Harrison, R. J. *J. Chem. Phys.* **1992**, *96*, 6796.

(51) Raghavachari, K.; Trucks, G. W.; Pople, J. A.; Head-Gordon, M. *Chem. Phys. Lett.* **1989**, *157*, 479.

(52) Martin, J. M. L.; Uzan, O. *Chem. Phys. Lett.* **1998**, *282*, 16.

(53) Werner, H.-J.; Knowles, P. J.; Lindh, R.; Manby, F. R.; Schütz, M.; Celani, P.; Korona, T.; Rauhut, G.; Amos, R. D.; Bernhardsson, A.; Berning, A.; Cooper, D. L.; Deegan, M. J. O.; Dobbyn, A. J.; Eckert, F.; Hampel, C.; Hetzer, G.; Lloyd, A. W.; McNicholas, S. J.; Meyer, W.; Mura, M. E.; Nicklass, A.; Palmieri, P.; Pitzer, R.; Schumann, U.; Stoll, H.; Stone, A. J.; Tarroni, R.; Thorsteinsson, T. *Molpro, A Package of Ab Initio Programs*, version 2008.1; University College Cardiff Consultants Limited: Cardiff, U.K., 2008. See http://www.molpro.net.

(54) Truhlar, D. G.; Garrett, B. C.; Klippenstein, S. J. *J. Phys. Chem.* **1996**, *31*, 12771.

(55) Klippenstein, S. J. *J. Chem. Phys.* **1992**, *96*, 367.

(56) Harding, L. B.; Georgievskii, Y.; Klippenstein, S. J. *J. Phys. Chem. A* **2005**, *109*, 4646.

(57) Klippenstein, S. J.; Georgievskii, Y.; Harding, L. B. *Phys. Chem. Chem. Phys.* **2006**, *8*, 1133.

(58) Bowman, C. T. *Combust. Flame* **1975**, *25*, 343.

(59) Burcat, A.; Ruscic, B. *Third Millennium Ideal Gas and Condensed Phase Thermochemical Database for Combustion with Updates from Active Thermochemical Tables*; Report ANL-05/20 and TAE 960; Argonne National Laboratory: Argonne, IL, 2005.

(60) Baulch, D. L.; Cobos, C. J.; Cox, R. A.; Esser, C.; Frank, P.; Just, T.; Kerr, J. A.; Pilling, M. J.; Troe, J.; Walker, R. W.; Warnatz, J. *J. Phys. Chem. Ref. Data* **1992**, *21*, 411. Baulch, D. L.; Cobos, C. J.; Cox, R. A.; Frank, P.; Hayman, G.; Just, T.; Kerr, J. A.; Murrells, T.; Pilling, M. J.; Troe, J.; Walker, R. W.; Warnatz, J. *J. Phys. Chem. Ref. Data* **1994**, *23*, 847.

(61) Tsang, W.; Hampson, W. F. *J. Phys. Chem. Ref. Data* **1986**, *15*, 1087. Tsang, W. *J. Phys. Chem. Ref. Data* **1987**, *16*, 471.

JP1047002